ACS Energy LETTERS

http://pubs.acs.org/journal/aelccp

Balancing Ion Diffusion-Reduction in Chlorine-Free Electrolytes Enables Long-Life Mg Metal Batteries

Juncai Long, Yi Liu, Wenwei Zhang, Ge Zhang, Pei Liu, Lianmeng Cui, Cheng Zhou, Jingke Ren, Ze He,* Qinyou An,* and Liqiang Mai*

Cite This: *ACS Energy Lett.* 2024, 9, 5019−5026

Read Online

ACCESS | Metrics & More | Article Recommendations | Supporting Information

ABSTRACT: **Homogeneous Mg plating/stripping behaviors have been widely recognized as the distinct advantage of rechargeable Mg metal batteries over other metal batteries. However, the rapid degradation mechanism of the Mg anode in practical chlorine-free electrolytes remains unclear. Herein, we reveal that the imbalance between Mg^{2+} diffusion and reduction rates during Mg plating is the main cause of uneven Mg deposition in a $Mg(HFIP)_2$ electrolyte, eventually resulting in cell short-circuits. We addressed this challenge by introducing a bulky tetrabutylammonium borohydride ($TBABH_4$) additive in the electrolyte. In detail, the uniform coverage of TBA^+ cations on the Mg anode surface regulates the Mg^{2+} reduction rate, ensuring homoepitaxy of the deposited Mg along the thermodynamically stable (002) crystal plane. Consequently, both Mg||Mg symmetrical cells and Mg||Mo_6S_8 full cells demonstrated doubled cycling stability and reduced overpotential. This work shed new light on stabilizing chlorine-free Mg metal batteries by balancing the ion diffusion-reduction rates.**

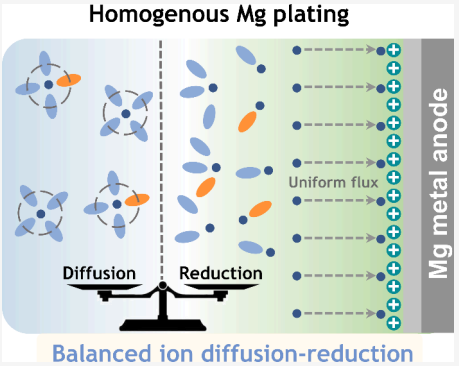

The adoption of metal anodes is expected to lead to high-energy rechargeable batteries due to their intrinsic high theoretical capacities and low redox potentials.[1−4] Despite these intriguing features, the ubiquitous dendrite growth issue leads to short circuits or thermal runaway in metal batteries. Uniform metal deposition is vital for battery long-term cyclability.[5] Among numerous metal anodes, deposited magnesium (Mg) atoms exhibit the lowest diffusion barrier, facilitating easier atom movement and yielding a homogeneous three-dimensional deposition morphology, rather than the rough surface associated with one-dimensional dendritic formation.[6] Therefore, rechargeable Mg metal batteries (RMBs) are widely recognized as one of the safest next-generation energy storage systems.[7−13]

Extensive research has revealed that electrodeposited Mg can maintain a homogeneous morphology over a board operational range ($\leq$5 mA cm^{-2} and 6 mAh cm^{-2}) in chlorine-containing electrolytes.[14−16] Nevertheless, the challenge of Mg−Cl complexes' co-insertion and the intrinsic low oxidative stability of these electrolytes constrain their application.[17,18] The development of chlorine-free Mg electrolytes is imminent. Our recently reported chlorine-free $Mg(HFIP)_2$ electrolyte demonstrates highly efficient Mg stripping/plating and outstanding cathode compatibility.[19] Unfortunately, chlorine-free Mg electrolytes normally demonstrate a limited cycle life (less than 500 h).[19−23] This could be attributed to the dendritic growth behavior of the Mg metal anode in these electrolytes.[24] According to the classical Sand's time model[25] and space-charge theory,[26,27] dendrite growth is mainly dominated by the cation concentration on the anode surface and the electric field distribution at the deposition sites. During the electrodeposition process, cations migrate to the anode surface under an applied electric field and undergo continuous reduction. Upon depletion of cations at the interface, the emergence of a charge-concentrated region facilitates the formation of a strong electric field that induces dendrite growth.[28]

Compared to monovalent Li^+, divalent Mg^{2+} normally shows a slower ionic conductivity in electrolytes.[29] In chlorine-containing electrolytes, the formation of a chlorine-rich interface not only promotes reversible Mg plating/stripping but also restricts the Mg electrodeposition rate due to the high

Received: August 7, 2024
Revised: September 12, 2024
Accepted: September 17, 2024

https://doi.org/10.1021/acsenergylett.4c02162
ACS Energy Lett. 2024, 9, 5019−5026

Scheme 1. Schematic of the Mg Deposition Model in (a) Chlorine-Containing Electrolytes and (b) Chlorine-Free Electrolytes

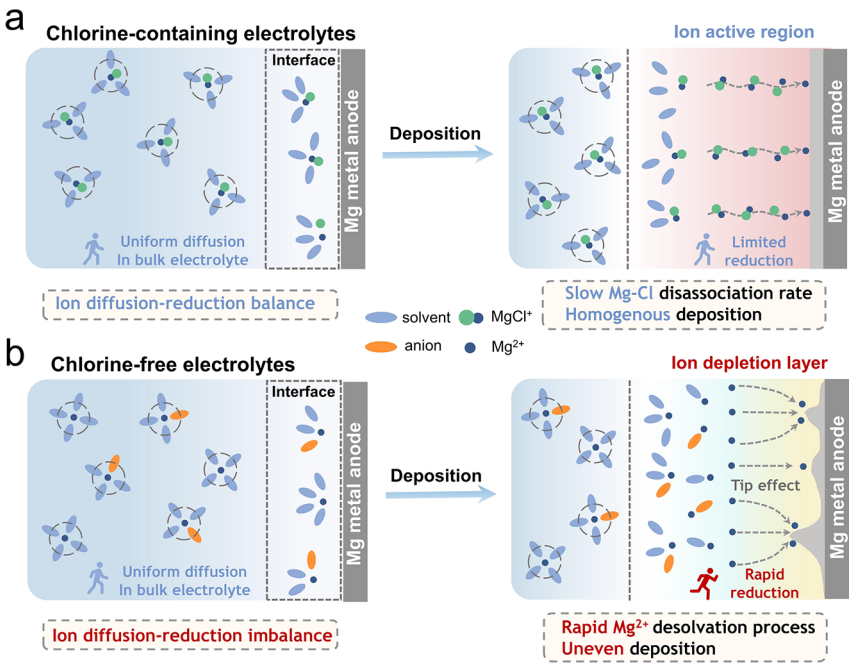

dissociation energy barrier of the Mg−Cl complexes.[30,31] Consequently, the Mg^{2+} diffusion rate is comparable with the reduction rate, leading to homogeneous plating morphology (Scheme 1a).[14] On the contrary, in chlorine-free electrolytes, the easier desolvation process of Mg^{2+} results in rapid cation consumption on the anode interface, thereby forming an ion depletion layer and inducing inhomogeneous nucleation−growth. The imbalance between Mg^{2+} diffusion and reduction eventually leads to uneven Mg deposition (Scheme 1b). Therefore, balancing the ion diffusion-reduction rates in chlorine-free electrolytes is essential to achieving uniform Mg plating. However, to the best of our knowledge, this has not been investigated.

In this work, we balance the Mg^{2+} diffusion-reduction rates by introducing bulky tetrabutylammonium borohydride ($TBABH_4$) molecules in chlorine-free $Mg(HFIP)_2$ electrolytes. The preferential adsorption of TBA^+ cations on the Mg anode surface can serve as a buffer layer for Mg^{2+} reduction. We investigate the morphology evolution and interface microenvironment change during the Mg plating process by in situ optical microscopy, in situ Raman spectra, DFT calculations, finite element method simulations, etc. Our findings suggest that this buffer layer can regulate the reduction rate through a self-adapting electrostatic interaction force and steric hindrance. Benefiting from the balanced ion diffusion-reduction processes, the diffusion-controlled random deposition mode was inhibited, thereby contributing to the sustained homoepitaxial growth of the deposited metal on the (002) oriented Mg anode substrate. Consequently, the Mg||Mg symmetrical cells and the Mg metal full cells using the modified electrolyte exhibit improved cycle life and reduced overpotential.

Chlorine-free $Mg(HFIP)_2$ electrolytes demonstrate a wide electrochemical window and a direct Mg^{2+} storage mechanism; however, they exhibit inherently low ionic conductivity (~0.3 mS cm^{-1}).[19] Since the rate of Mg^{2+} reduction is not constrained by the sluggish Mg−Cl bond dissociation in chlorine-free electrolytes, the rate of Mg^{2+} consumption at the anode interface significantly surpasses their diffusion rate. This diffusion-reduction mismatch leads to the formation of a Mg^{2+} depletion layer, resulting in the dendrite growth of Mg. In the modified electrolyte, TBA^+ cations preferentially adsorb at the interface to form a cationic shielding layer that reconstructs the local electric field. Specifically, during the deposition process, protuberances on the anode can adsorb more TBA^+ cations due to their higher local current density.[32] This suggests that a self-adapting TBA^+ adsorption layer could form on an uneven Mg foil, where the tips generate stronger electrostatic repulsion than uniform areas. On the one hand, this self-adapting buffer layer reduces the Mg^{2+} reduction rate to match the sluggish Mg^{2+} diffusion rate, leading to uniform Mg deposition without the formation of an Mg^{2+} depletion layer. On the other hand, the strong electrostatic repulsion at the tips suppresses Mg deposition in these areas until they become even (Figure 1a). In situ optical microscopy provides a more intuitive comparison, revealing scattered dark Mg grains that become apparent after 10 min of plating in the $Mg(HFIP)_2$ electrolyte. As the plating time increased, these initial protuberances gradually developed into moss-like dendrites. This localized Mg deposition pattern exacerbates self-enhancing nucleation growth, consequently accelerating the deterioration of Mg anodes (Figure 1b). However, the self-adapting electrostatic shield layer in our $TBA^+/Mg(HFIP)_2$ electrolyte regulates the reduction rate of Mg^{2+} and limits the sustained growth of initial Mg deposits, leading to a dendrite-free platting morphology over 60 min (Figure 1c).

Moreover, we reveal the regulated Mg stripping morphology in the modified electrolyte using a confocal laser scanning microscope (CLSM). The Mg anode cycled in the blank electrolyte exhibits an average surface roughness of 2.35 μm along with massive stripping pits (Figure 1d). In contrast, significantly suppressed stripping pit growth with low roughness (~0.8 μm) was observed on the Mg anode cycled in the $TBA^+/Mg(HFIP)_2$ electrolyte (Figure 1e). The suppression of uneven plating and stripping behaviors can lead to a quantum leap in the lifetime of Mg anodes, which we will investigate in more detail in the following sections.[33]

https://doi.org/10.1021/acsenergylett.4c02162
ACS Energy Lett. 2024, 9, 5019−5026

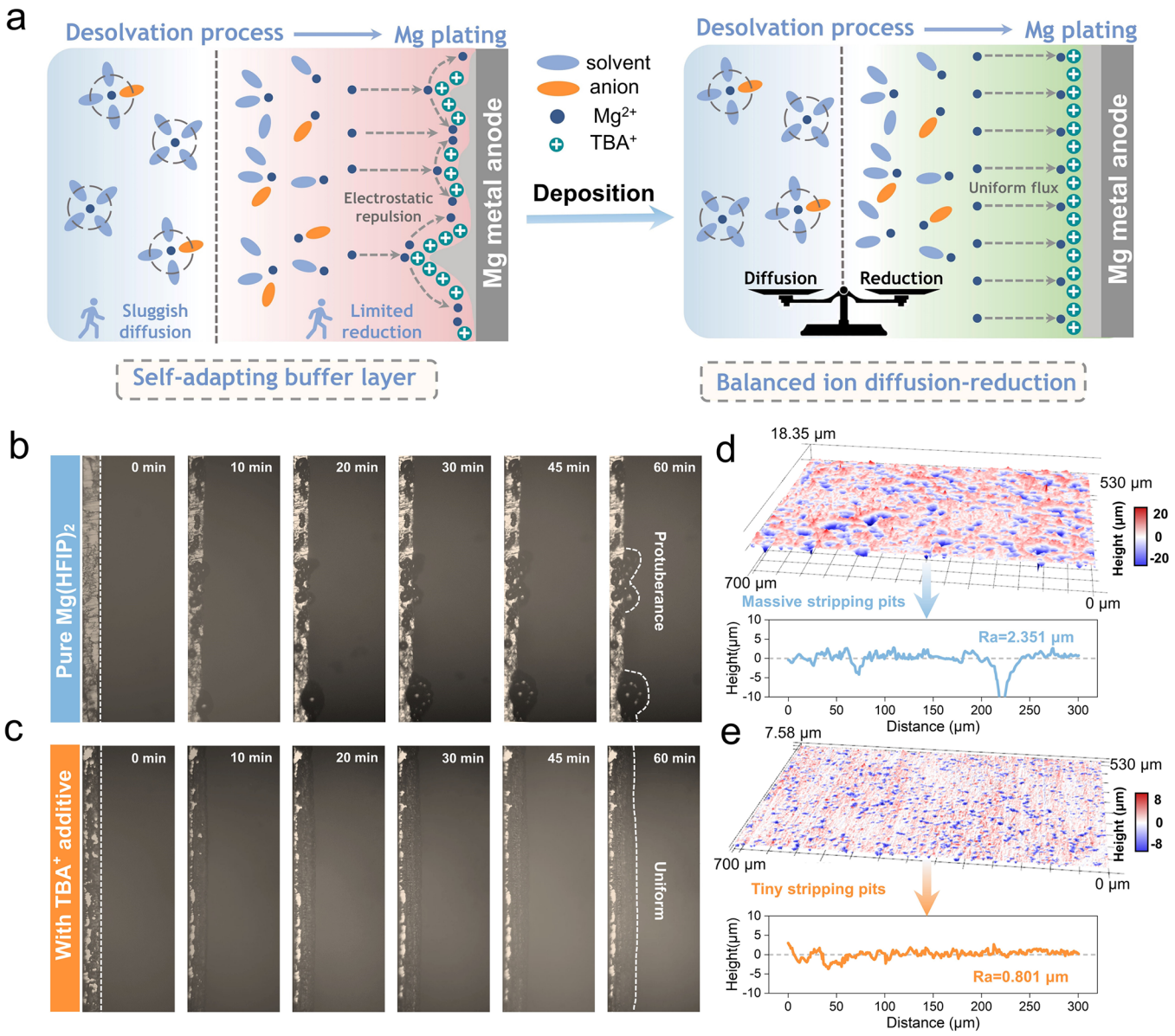

Figure 1. (a) Schematic illustration of the effect of TBA^+ cations on the Mg deposition process. (b) In situ microscopy images of the Mg plating process in $Mg(HFIP)_2$ electrolytes and (c) $TBA^+/Mg(HFIP)_2$ electrolytes. CLSM images and the corresponding surface roughness curve of Mg anodes after being stripped in (d) $Mg(HFIP)_2$ electrolytes and (e) $TBA^+/Mg(HFIP)_2$ electrolytes.

To gain deeper insight into how additive molecules influence Mg deposition, our research focused further on the solvation structure and the electrode−electrolyte interface. The negligible changes in Fourier transform infrared (FTIR) and Raman spectra of the $Mg(HFIP)_2$ electrolytes with or without TBA^+ cations suggest that trace amounts of additives do not directly alter the solvation structure of Mg^{2+} (Figures S1 and S2).[34,35] In addition, the ionic conductivity of electrolytes remained nearly unchanged (Figure S3). The overlapping and transition of electron clouds in 3D adsorption configurations suggest that TBA^+ cations show pronounced charge transfer on three main Mg crystal planes (Figure 2a−c and Figure S4). In addition, the adsorption energy of TBA^+ cations on various Mg crystal planes is −3.27 eV (002), −3.03 eV (100), and −2.98 eV (101), respectively, which are significantly lower than that of Mg to Mg^{2+} (ca. −1 eV; Figure 2d). These calculation results indicate that TBA^+ cations preferentially adsorb on the Mg metal surface, forming a Mg^{2+} reduction buffer layer.[36]

In situ Raman spectra provide compelling evidence of TBA^+ adsorption on the Mg metal anode. During the Mg plating and stripping processes, only $HFIP^-$ anions (740 cm^{-1}) and DME solvent (816, 849, and 879 cm^{-1}) signals were detected on the Mg surface in the blank $Mg(HFIP)_2$ electrolytes (Figure 2e).[19] For the TBA^+ modified electrolyte, we observed the emergence of two additional peaks (1364 and 1398 cm^{-1}) corresponding to TBA^+ adsorption (Figure 2f).[37,38] Notably, these two adsorption peaks gradually diminished and then recovered during the charge/discharge switching. This happens because reversing the electric field direction desorbs certain TBA^+ cations, and the peak intensities of adsorbed TBA^+ cations rebounded when the Mg plating/stripping process stabilized. Time-of-flight secondary ion mass spectrometry (TOF-SIMS) 3D visualizations of cycled Mg anodes in two electrolytes were in agreement with the aforementioned results. Strong signals for the decomposed TBA^+ cations ($C_2H_2^+$, $C_3H_7^+$, CH^-, C^-, and $NC_4H_9^-$) were observed in the normalized depth profiles

https://doi.org/10.1021/acsenergylett.4c02162
ACS Energy Lett. 2024, 9, 5019−5026

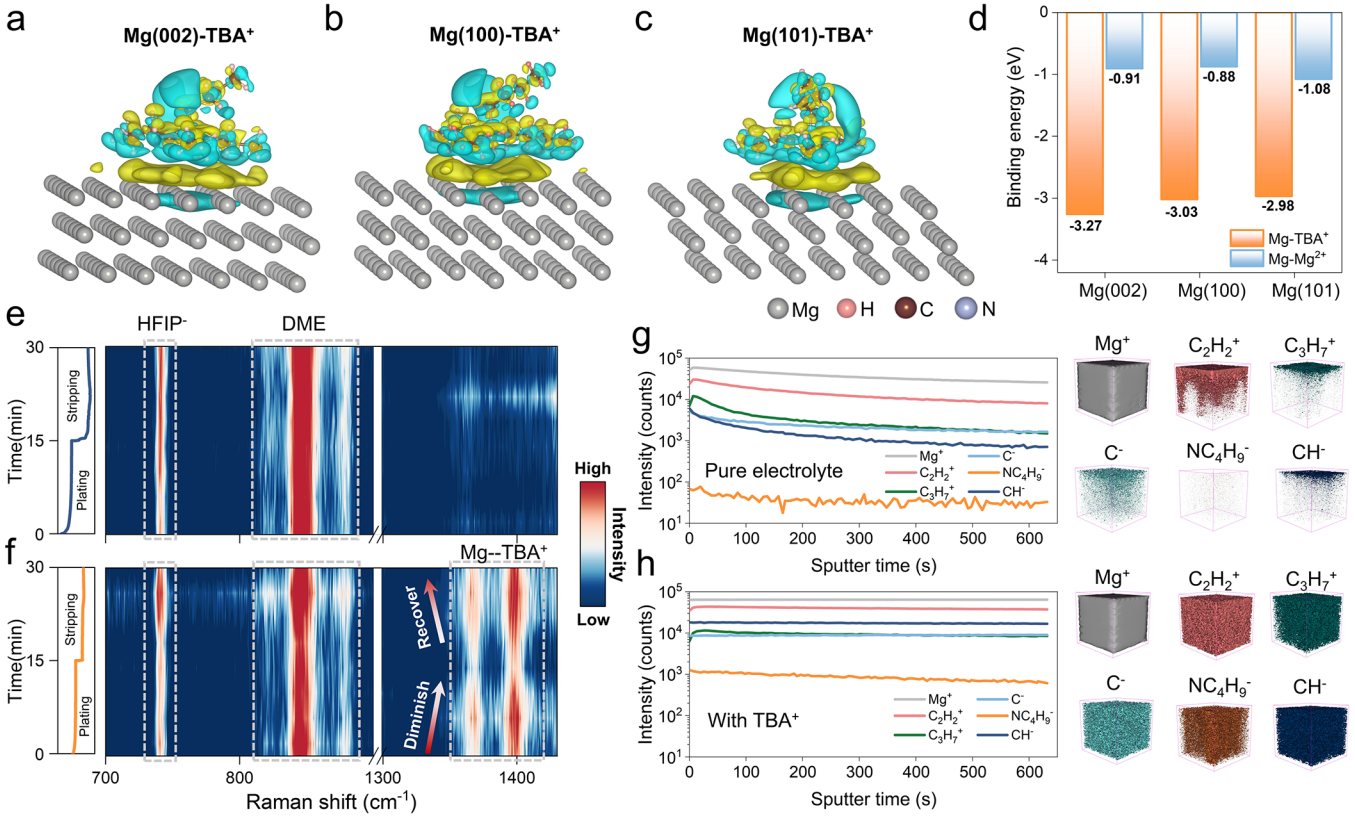

Figure 2. Electron density difference at interfaces for (a) Mg (002), (b) Mg (100), and (c) Mg (101) crystal planes in conjunction with TBA^+ cations. The bottom three layers of the Mg atoms are fixed during calculation. The green area indicates electron consumption, while the yellow area indicates electron accumulation. (d) The binding energy of Mg^{2+} and TBA^+ cations on various Mg crystal planes. (e) In situ 2D Raman spectra and corresponding galvanostatic charge/discharge (GCD) profiles of $Mg(HFIP)_2$ electrolytes and (f) $TBA^+/Mg(HFIP)_2$ electrolytes during the plating/stripping process. (g) TOF-SIMS 3D rendering models and depth profiles in the positive and negative modes of the Mg metal anodes cycled in (g) $Mg(HFIP)_2$ electrolytes and (h) $TBA^+/Mg(HFIP)_2$ electrolytes.

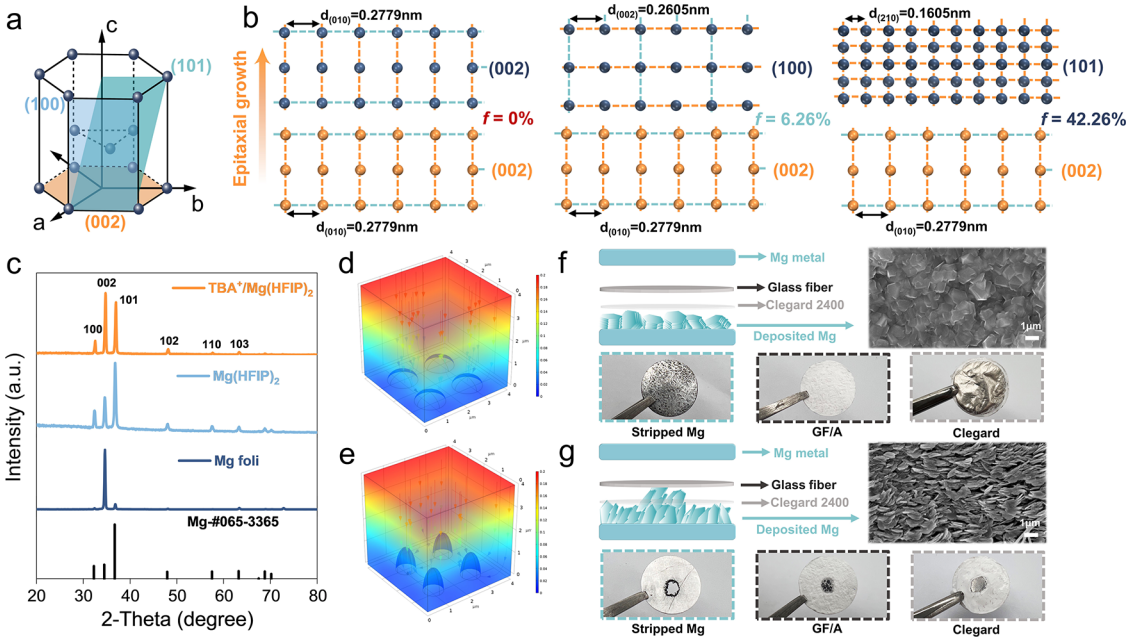

Figure 3. (a) The illustration of the hexagonal close-packed (hcp) structure of Mg. (b) The lattice mismatch of Mg(002), Mg(100), and Mg(101) to Mg(002) crystal planes, respectively. (c) XRD patterns of Mg foil and Mg anode cycled in $Mg(HFIP)_2$ and $TBA^+/Mg(HFIP)_2$ electrolytes, respectively. (d) The simulation of electric field distribution in $TBA^+/Mg(HFIP)_2$ and (e) $Mg(HFIP)_2$ electrolytes. Schematics of electrode structures, SEM images of Mg electrode and photographic images of Mg anode, GF separators, and Clegard 2400 membranes after plating in (f) $TBA^+/Mg(HFIP)_2$ and (g) $Mg(HFIP)_2$ electrolytes.

https://doi.org/10.1021/acsenergylett.4c02162
ACS Energy Lett. 2024, 9, 5019−5026

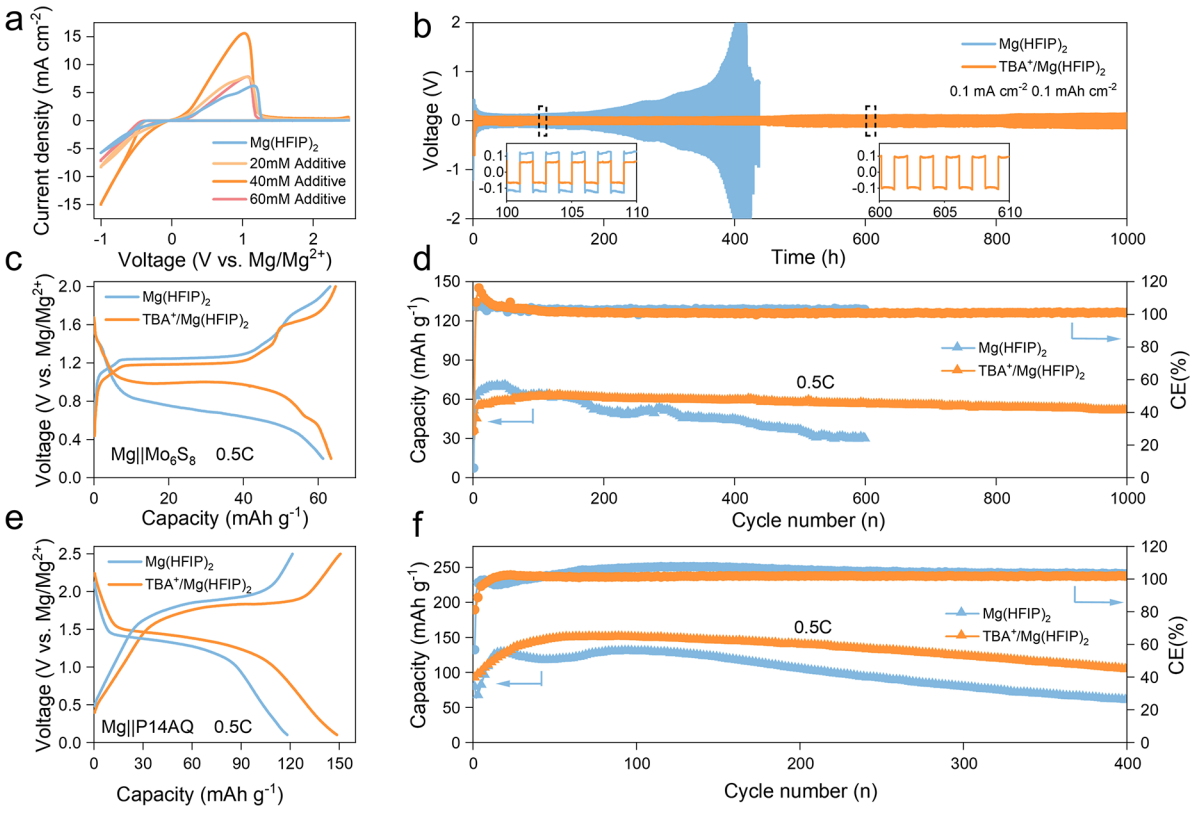

Figure 4. (a) Cyclic voltammograms of the Mg plating/stripping process in $Mg(HFIP)_2$ electrolyte with different concertation additives at 25 mV s^{-1}. (b) Galvanostatic cycling of Mg||Mg symmetrical cells using $Mg(HFIP)_2$ and $TBA^+/Mg(HFIP)_2$ electrolytes with a current density of 0.1 mA cm^{-2} and a capacity of 0.1 mAh cm^{-2}. (c) Charge−discharge curves of Mg||Mo_6S_8 cells at 0.5 C (1 C = 128 mA g^{-1}) and (d) corresponding cycle performance in $Mg(HFIP)_2$ and $TBA^+/Mg(HFIP)_2$ electrolytes. (e) Charge−discharge curves of Mg||P14AQ cells at 0.5 C (1 C = 260 mA g^{-1}) and (f) corresponding cycle performance in $Mg(HFIP)_2$ and $TBA^+/Mg(HFIP)_2$ electrolytes.

of the Mg anode cycled in $TBA^+/Mg(HFIP)_2$ electrolyte (Figure 2h). In contrast, when the Mg anode cycled in pure $Mg(HFIP)_2$ electrolyte, only signals originating from solvent and anions decomposition are present (Figure 2g). Both theoretical calculations and experimental results confirm the formation of a TBA^+ cation adsorption layer on the Mg anode surface in the $TBA^+/Mg(HFIP)_2$ electrolytes. This layer balances the Mg^{2+} diffusion-reduction rates and leads to uniform Mg plating. However, an additional investigation into its underlying effects is necessary.

Previous studies on electrolyte additives have mainly focused on regulating solvation structures and constructing solid electrolyte interfaces (SEIs).[39,40] However, neither the solvation structure nor SEI formation was changed in our TBA^+ modified electrolyte (Figures S5 and S6). These observations warrant a closer analysis of the additive's effects in other aspects.

Hexagonal Mg metal, characterized by a space group of *P*63/*mmc*, whose Mg(101) and Mg(100) crystal plane orientations are vertically aligned to the current collector, leading to inhomogeneous deposits and additional side reactions with the electrolyte.[41] In contrast, Mg(002) planes typically stack parallel to the electrode surface, promoting higher planar packing density and resistance to Mg corrosion (Figure 3a). Therefore, preferential growth of the Mg(002) plane is crucial for long-life Mg anodes.[42] It is worth noting that the commonly used Mg foil delivers a textured crystal structure with a predominantly exposed (002) crystal plane (Figure 3c). Under ideal deposition conditions, the epitaxial growth of deposited Mg metal along the (002) crystal plane is thermodynamically the most favorable due to zero lattice mismatch.[43] In contrast, depositing Mg(100) and Mg(101) planes on Mg(002) is thermodynamically unfavorable due to the large mismatches (6.26% and 42.26%, respectively; Figure 3b).[44,45] However, we observed that Mg(101) deposition is predominant on commercial Mg foil in the $Mg(HFIP)_2$ electrolyte. The peak intensity ratio of deposited Mg closely matches the predicted ratio for randomly oriented Mg grains (I_{002}:I_{101} = 0.27, reference code 03−065−3365).[46,47] This is due to the imbalance between Mg^{2+} ion diffusion and reduction during plating, under which conditions the Mg nucleation−growth is mainly controlled by ionic diffusion kinetics.[28] In contrast, the I_{002}:I_{101} ratio of deposited Mg increased from 0.27 to 1.18 in our TBA^+ modified electrolyte. The preferential deposition of the Mg(002) plane demonstrates a substrate-controlled plating process, indicating an optimized Mg^{2+} diffusion-reduction balance (Figure S7). Despite the presence of some undesired (100) and (101) plane deposition, the predominant Mg(002) plane plating could potentially benefit the long-term durability of the Mg anode.

Finite element method (FEM) simulations were conducted to further validate the role of the cation buffer layer in regulating the charge transfer and Mg nucleation behaviors. In contrast to concentrated electric field distribution and sharp protuberances observed in the blank electrolyte (Figure 3e), the introduced TBA^+ cations reconstruct the microenvironment on the deposited Mg surface, yielding a homogeneous

https://doi.org/10.1021/acsenergylett.4c02162
ACS Energy Lett. 2024, 9, 5019−5026

deposition morphology (Figure 3d, Figure S8). To better demonstrate the morphology and crystal orientation optimization of Mg plating in our $TBA^+/Mg(HFIP)_2$ electrolytes, we performed post-mortem analysis of cycled Mg anodes in different electrolytes. We used an extra Celgard 2400 membrane between the Mg foil and the glass fiber (GF) separator to mitigate surface damage during cell disassembly. Scanning electron microscopy (SEM) images demonstrate the sheet-stacked Mg deposition morphology in our modified electrolytes, corresponding to typical horizontal (002) Mg plating (Figure 3f). In comparison, the Mg foil cycled in the blank $Mg(HFIP)_2$ electrolyte shows a loose morphology with vertical Mg grains (Figure 3g). Moreover, photographs of the Mg foils and separators after cycling demonstrate the severely uneven plating/stripping behavior in blank electrolytes at the macro level (Figure 3g). After cycling at a relatively low areal capacity of 2 mAh cm^{-2}, we observed the perforation of stripped Mg, indicating localized Mg plating/stripping behavior. Correspondingly, locally plated Mg aggregated and punctured the Celgard membrane, leaving substantial amounts of "dead" Mg residue in the glass fiber separator. On the contrary, the Mg foil cycled in the $TBA^+/Mg(HFIP)_2$ electrolyte demonstrates uniform plating/stripping behavior. All areas of the Mg foil react evenly, and no Mg was observed growing inside the GF separator.

Mg||SS asymmetrical cells and Mg||Mg symmetrical cells were assembled to assess the electrochemical performance of the $TBA^+/Mg(HFIP)_2$ electrolyte. As illustrated in Figure 4a, the increase in the TBA^+ concentration in the $Mg(HFIP)_2$ electrolyte can enhance the Mg plating/stripping kinetics. However, the Mg plating/stripping kinetics was significantly inhibited when the TBA^+ concentration reached 60 mM, presumably due to the excessively suppressed Mg reduction rate caused by the thick TBA^+ adsorption layer formed on the Mg surface. In addition, excessive additives can also decrease the oxidation stability of the electrolyte (Figure S9). Consequently, 40 mM TBA^+ was chosen as the optimal concentration for rapid Mg plating/stripping. As a result, the Mg symmetrical cells containing 40 mM $TBABH_4$ additive demonstrate the lowest voltage hysteresis (70 mV) and the longest cycling lifespan (1000 h) compared to those using a blank $Mg(HFIP)_2$ electrolyte, 20 mM $TBABH_4$, and 60 mM $TBABH_4$ (Figure 4b and Figure S10). Even under a relatively high current density of 2 mA cm^{-2}, a decent polarization (350 mV) is maintained (Figure S11). In addition, improved Coulombic efficiency and reduced impedance were observed in the Mg cells cycled in a 40 mM TBA^+ modified electrolyte (Figures S12 and S13). The facilitated charge transfer kinetics observed in electrochemical impedance spectroscopy may also originate from the additive's BH_4^- anions, which remove H_2O from the electrolyte and minimize the surface passivation.[39]

To evaluate the practical applicability of the $TBA^+/Mg(HFIP)_2$ electrolyte, we assembled Mg metal full cells using a classical Mo_6S_8 cathode (Figure S14), organic P14AQ cathode (Figure S15), and spinel $MgMn_2O_4$ cathode (Figures S16 and S17). The Mg||Mo_6S_8 full cells with 40 mM TBA^+ additives show reduced charge/discharge polarization (Figure 4c) and a doubled cycling lifetime compared to those using a blank electrolyte, enabling a 92% capacity retention over 1000 cycles (Figure 4d). It is worth noting that the Mg||Mo_6S_8 full cells deliver decreased open-circuit voltages with the TBA^+ additives, further confirming the adsorption of TBA^+ cations on the Mg anode (Figure S18). Similar improvements were also observed in high-voltage organic Mg||P14AQ full cells. As illustrated in Figure 4e,f, an average discharge voltage of ~1.35 V and a capacity retention of 70% (relative to peak capacity) after 400 cycles were demonstrated by using our $TBA^+/Mg(HFIP)_2$ electrolyte. These results highlight the good compatibility of the TBA^+ additive with both Mg anodes and various cathodes, making it a viable additive for practical RMBs.

In summary, we developed a strategy to balance the Mg^{2+} diffusion and reduction rates in the chlorine-free $Mg(HFIP)_2$ electrolyte by introducing a TBA^+ additive with a high Mg affinity. The preferential adsorption of TBA^+ cations on the Mg anode surface forms a dynamic electrostatic shield layer. This layer slows the Mg^{2+} reduction rate through electrostatic repulsion and steric hindrance, aligning it with the relatively slow Mg^{2+} diffusion rate. The balanced Mg^{2+} diffusion-reduction processes guarantee the preferential growth of the most thermodynamically stable Mg(002) crystal planes, enabling uniform Mg plating/stripping morphologies in chlorine-free $Mg(HFIP)_2$ electrolytes. Consequently, both the Mg symmetrical cells and full cells with an optimized concentration of TBA^+ additives demonstrate a doubled cycling lifespan and reduced polarizations. Moreover, our electrolyte demonstrates excellent compatibility with both the inorganic and organic cathodes, achieving 92% capacity retention over 1000 cycles and 70% capacity retention over 400 cycles in the Mg||Mo_6S_8 and Mg||P14AQ full cells, respectively. Our research highlights the critical role of balancing diffusion-reduction rates in achieving stable Mg plating/stripping and proposes an effective interface regulation strategy for practical Mg electrolyte design.

■ ASSOCIATED CONTENT

Supporting Information

The Supporting Information is available free of charge at https://pubs.acs.org/doi/10.1021/acsenergylett.4c02162.

Experimental procedures including materials preparation, characterization, electrochemical measurements, COMSOL simulations, and DFT calculations method; additional materials characterization, and electrochemical data (PDF)

■ AUTHOR INFORMATION

Corresponding Authors

Ze He − *State Key Laboratory of Advanced Technology for Materials Synthesis and Processing, Wuhan University of Technology, Wuhan 430070, People's Republic of China; Institute for Manufacturing, Department of Engineering, University of Cambridge, Cambridge CB3 0FS, United Kingdom*; Email: He816414@163.com

Qinyou An − *State Key Laboratory of Advanced Technology for Materials Synthesis and Processing, Wuhan University of Technology, Wuhan 430070, People's Republic of China; Hubei Longzhong Laboratory, Wuhan University of Technology (Xiangyang Demonstration Zone), Xiangyang 441000, People's Republic of China*; orcid.org/0000-0003-0605-4942; Email: anqinyou86@whut.edu.cn

Liqiang Mai − *State Key Laboratory of Advanced Technology for Materials Synthesis and Processing, Wuhan University of Technology, Wuhan 430070, People's Republic of China; Hubei Longzhong Laboratory, Wuhan University of Technology (Xiangyang Demonstration Zone), Xiangyang*

https://doi.org/10.1021/acsenergylett.4c02162
ACS Energy Lett. 2024, 9, 5019−5026

441000, People's Republic of China; Email: mlq518@whut.edu.cn

Authors

Juncai Long − *State Key Laboratory of Advanced Technology for Materials Synthesis and Processing, Wuhan University of Technology, Wuhan 430070, People's Republic of China*

Yi Liu − *State Key Laboratory of Advanced Technology for Materials Synthesis and Processing, Wuhan University of Technology, Wuhan 430070, People's Republic of China*

Wenwei Zhang − *State Key Laboratory of Advanced Technology for Materials Synthesis and Processing, Wuhan University of Technology, Wuhan 430070, People's Republic of China*

Ge Zhang − *State Key Laboratory of Advanced Technology for Materials Synthesis and Processing, Wuhan University of Technology, Wuhan 430070, People's Republic of China*

Pei Liu − *State Key Laboratory of Advanced Technology for Materials Synthesis and Processing, Wuhan University of Technology, Wuhan 430070, People's Republic of China*

Lianmeng Cui − *State Key Laboratory of Advanced Technology for Materials Synthesis and Processing, Wuhan University of Technology, Wuhan 430070, People's Republic of China*

Cheng Zhou − *State Key Laboratory of Advanced Technology for Materials Synthesis and Processing, Wuhan University of Technology, Wuhan 430070, People's Republic of China*

Jingke Ren − *State Key Laboratory of Advanced Technology for Materials Synthesis and Processing, Wuhan University of Technology, Wuhan 430070, People's Republic of China*

Complete contact information is available at: https://pubs.acs.org/10.1021/acsenergylett.4c02162

Notes

The authors declare no competing financial interest.

■ ACKNOWLEDGMENTS

This work was supported by the National Key Research and Development Program of China (No. 2023YFB3809501), the National Natural Science Foundation of China (52172231), the Natural Science Foundation of Hubei Province (2022CFA087, 2024AFB040).

■ REFERENCES

(1) Liang, Y.; Dong, H.; Aurbach, D.; Yao, Y. Current status and future directions of multivalent metal-ion batteries. *Nat. Energy* **2020**, *5* (9), 646−656.

(2) Attias, R.; Salama, M.; Hirsch, B.; Goffer, Y.; Aurbach, D. Anode-Electrolyte Interfaces in Secondary Magnesium Batteries. *Joule* **2019**, *3* (1), 27−52.

(3) Zhao-Karger, Z.; Xiu, Y.; Li, Z.; Reupert, A.; Smok, T.; Fichtner, M. Calcium-tin alloys as anodes for rechargeable non-aqueous calcium-ion batteries at room temperature. *Nat. Commun.* **2022**, *13*, 3849.

(4) Wu, C.; Xue, L.; Xu, R.; Fan, J.; Chen, T.; Tang, W.; Cui, L.; Wang, A.; Dou, S. X.; Peng, C. Toward high-energy magnesium battery anode: recent progress and future perspectives. *Mater. Today Energy* **2024**, *40*, 101485.

(5) Hagopian, A.; Doublet, M.-L.; Filhol, J.-S. Thermodynamic origin of dendrite growth in metal anode batteries. *Energy Environ. Sci.* **2020**, *13* (12), 5186−5197.

(6) Jäckle, M.; Helmbrecht, K.; Smits, M.; Stottmeister, D.; Groß, A. Self-diffusion barriers: possible descriptors for dendrite growth in batteries? *Energy Environ. Sci.* **2018**, *11* (12), 3400−3407.

(7) Long, J.; Tan, S.; Wang, J.; Xiong, F.; Cui, L.; An, Q.; Mai, L. Revealing the Interfacial Chemistry of Fluoride Alkyl Magnesium Salts in Magnesium Metal Batteries. *Angew. Chem., Int. Ed.* **2023**, *62*, No. e202301934.

(8) Du, Y.; Chen, Y.; Tan, S.; Chen, J.; Huang, X.; Cui, L.; Long, J.; Wang, Z.; Yao, X.; Shang, B.; et al. Strong solvent coordination effect inducing gradient solid-electrolyte-interphase formation for highly efficient Mg plating/stripping. *Energy Storage Mater.* **2023**, *62*, 102939.

(9) Huang, X.; Tan, S.; Chen, J.; Que, Z.; Deng, R.; Long, J.; Xiong, F.; Huang, G.; Zhou, X.; Li, L.; Wang, J.; Mai, L.; Pan, F. Asymmetric SO3CF3–Grafted Boron-Center Anion Enables Boron-Containing Interphase for High-Performance Rechargeable Mg Batteries. *Adv. Funct. Mater.* **2024**, *34*, 2314146.

(10) Wu, C.; Shi, H.; Zhao, L.; Chen, X.; Zhang, X.; Zhang, C.; Yu, J.; Lv, Y.; Wei, R.; Gao, T.; Xie, J.; Yu, Y.; Liu, W. High-Performance Aqueous Zn2+/Al3+ Electrochromic Batteries based on Niobium Tungsten Oxides. *Adv. Funct. Mater.* **2023**, *33* (20), 2214886.

(11) He, B.; Ling, Y.; Wang, Z.; Gong, W.; Wang, Z.; Liu, Y.; Zhou, T.; Xiong, T.; Wang, S.; Wang, Y.; et al. Modulating selective interaction of NiOOH with Mg ions for high-performance aqueous batteries. *eScience* **2024**, 100293.

(12) Wen, T.; Deng, Y.; Qu, B.; Huang, G.; Song, J.; Xu, C.; Du, A.; Xie, Q.; Wang, J.; Cui, G.; et al. Re-envisioning the Key Factors of Magnesium Metal Anodes for Rechargeable Magnesium Batteries. *ACS Energy Lett.* **2023**, *8* (11), 4848−4861.

(13) Wen, T.; Qu, B.; Tan, S.; Huang, G.; Song, J.; Wang, Z.; Wang, J.; Tang, A.; Pan, F. Rational design of artificial interphase buffer layer with 3D porous channel for uniform deposition in magnesium metal anodes. *Energy Storage Mater.* **2023**, *55*, 816−825.

(14) Liu, X.; Du, A.; Guo, Z.; Wang, C.; Zhou, X.; Zhao, J.; Sun, F.; Dong, S.; Cui, G. Uneven Stripping Behavior, A Unheeded killer of Mg Anodes. *Adv. Mater.* **2022**, *34*, 2201886.

(15) Kwak, J. H.; Jeoun, Y.; Oh, S. H.; Yu, S.; Lim, J.-H.; Sung, Y.-E.; Yu, S.-H.; Lim, H.-D. Operando Visualization of Morphological Evolution in Mg Metal Anode: Insight into Dendrite Suppression for Stable Mg Metal Batteries. *ACS Energy Lett.* **2022**, *7*, 162−170.

(16) Wen, T.; Tan, S.; Li, R.; Huang, X.; Xiao, H.; Teng, X.; Jia, H.; Xiong, F.; Huang, G.; Qu, B.; et al. Large-Scale Integration of the Ion-Reinforced Phytic Acid Layer Stabilizing Magnesium Metal Anode. *ACS Nano* **2024**, *18* (18), 11740−11752.

(17) Dong, H.; Liang, Y.; Tutusaus, O.; Mohtadi, R.; Zhang, Y.; Hao, F.; Yao, Y. Directing Mg-Storage Chemistry in Organic Polymers toward High-Energy Mg Batteries. *Joule* **2019**, *3* (3), 782−793.

(18) Zhou, L.; Liu, Q.; Zhang, Z.; Zhang, K.; Xiong, F.; Tan, S.; An, Q.; Kang, Y. M.; Zhou, Z.; Mai, L. Interlayer-Spacing-Regulated VOPO4 Nanosheets with Fast Kinetics for High-Capacity and Durable Rechargeable Magnesium Batteries. *Adv. Mater.* **2018**, *30* (32), 1801984.

(19) Long, J.; Liu, Y.; He, Z.; Tan, S.; Xiong, F.; Xu, H.; Wang, W.; Zhang, G.; Yang, Z.; An, Q. Redesigning Solvation Structure toward Passivation-Free Magnesium Metal Batteries. *ACS Nano* **2024**, *18* (23), 15239−15248.

(20) Ren, W.; Wu, D.; NuLi, Y.; Zhang, D.; Yang, Y.; Wang, Y.; Yang, J.; Wang, J. An Efficient Bulky Mg[B(Otfe)4]2 Electrolyte and Its Derivatively General Design Strategy for Rechargeable Magnesium Batteries. *ACS Energy Lett.* **2021**, *6* (9), 3212−3220.

(21) Wang, F.; Hua, H.; Wu, D.; Li, J.; Xu, Y.; Nie, X.; Zhuang, Y.; Zeng, J.; Zhao, J. Solvent Molecule Design Enables Excellent Charge Transfer Kinetics for a Magnesium Metal Anode. *ACS Energy Lett.* **2023**, *8* (1), 780−789.

(22) Dong, H.; Tutusaus, O.; Liang, Y.; Zhang, Y.; Lebens-Higgins, Z.; Yang, W.; Mohtadi, R.; Yao, Y. High-power Mg batteries enabled by heterogeneous enolization redox chemistry and weakly coordinating electrolytes. *Nat. Energy* **2020**, *5* (12), 1043−1050.

(23) Zhao, W.; Pan, Z.; Zhang, Y.; Liu, Y.; Dou, H.; Shi, Y.; Zuo, Z.; Zhang, B.; Chen, J.; Zhao, X.; Yang, X. Tailoring Coordination in

Conventional Ether-Based Electrolytes for Reversible Magnesium-Metal Anodes. *Angew. Chem., Int. Ed.* **2022**, *61* (30), No. e202205187.
(24) Davidson, R.; Verma, A.; Santos, D.; Hao, F.; Fincher, C.; Xiang, S.; Van Buskirk, J.; Xie, K.; Pharr, M.; Mukherjee, P. P.; et al. Formation of Magnesium Dendrites during Electrodeposition. *ACS Energy Lett.* **2019**, *4* (2), 375−376.
(25) Sand, H. J.S. On the concentration at the electrodes in a solution, with special reference to the liberation of hydrogen by electrolysis of a mixture of copper sulphate and sulphuric acid. *Philos. Mag.* **1901**, *1* (1), 45−79.
(26) Fleury, V.; Chazalviel, J. N.; Rosso, M.; Sapoval, B. The role of the anions in the growth speed of fractal electrodeposits. *J. Electroanal. Chem. Interfacial Electrochem.* **1990**, *290* (1), 249−255.
(27) Chazalviel, J. N. Electrochemical aspects of the generation of ramified metallic electrodeposits. *Phys. Rev. A* **1990**, *42* (12), 7355−7367.
(28) Zou, P.; Sui, Y.; Zhan, H.; Wang, C.; Xin, H. L.; Cheng, H.-M.; Kang, F.; Yang, C. Polymorph Evolution Mechanisms and Regulation Strategies of Lithium Metal Anode under Multiphysical Fields. *Chem. Rev.* **2021**, *121* (10), 5986−6056.
(29) Roy, A.; Sotoudeh, M.; Dinda, S.; Tang, Y.; Kübel, C.; Groß, A.; Zhao-Karger, Z.; Fichtner, M.; Li, Z. Improving rechargeable magnesium batteries through dual cation co-intercalation strategy. *Nat. Commun.* **2024**, *15* (1), 492.
(30) Attias, R.; Chae, M. S.; Dlugatch, B.; Oliel, M.; Goffer, Y.; Aurbach, D. The Role of Surface Adsorbed Cl- Complexes in Rechargeable Magnesium Batteries. *ACS Catal.* **2020**, *10* (14), 7773−7784.
(31) Barile, C. J.; Barile, E. C.; Zavadil, K. R.; Nuzzo, R. G.; Gewirth, A. A. Electrolytic Conditioning of a Magnesium Aluminum Chloride Complex for Reversible Magnesium Deposition. *J. Phys. Chem. C* **2014**, *118* (48), 27623−27630.
(32) Yuan, Y.; Pu, S. D.; Perez-Osorio, M. A.; Li, Z.; Zhang, S.; Yang, S.; Liu, B.; Gong, C.; Menon, A. S.; Piper, L. F. J.; Gao, X.; Bruce, P. G.; Robertson, A. W. Diagnosing the Electrostatic Shielding Mechanism for Dendrite Suppression in Aqueous Zinc Batteries. *Adv. Mater.* **2024**, *36* (9), 2307708.
(33) Liu, X.; Wang, G.; Lv, Z.; Du, A.; Dong, S.; Cui, G. A Perspective on Uniform Plating Behavior of Mg Metal Anode: Diffusion Limited Theory versus Nucleation Theory. *Adv. Mater.* **2024**, *36* (9), 2306395.
(34) Wang, S.; Wang, K.; Zhang, Y.; Jie, Y.; Li, X.; Pan, Y.; Gao, X.; Nian, Q.; Cao, R.; Li, Q.; Jiao, S.; Xu, D. High-entropy Electrolyte Enables High Reversibility and Long Lifespan for Magnesium Metal Anodes. *Angew. Chem., Int. Ed.* **2023**, *62* (31), No. e202304411.
(35) Wang, W.; Ju, S.; Zhang, H.; Zhou, X.; Yu, X. Synchronous regulation on solvation structure and interface engineering to enable reversible magnesium metal batteries. *Energy Storage Mater.* **2024**, *70*, 103493.
(36) Hu, Z.; Zhang, F.; Zhao, Y.; Wang, H.; Huang, Y.; Wu, F.; Chen, R.; Li, L. A Self-Regulated Electrostatic Shielding Layer toward Dendrite-Free Zn Batteries. *Adv. Mater.* **2022**, *34* (37), 2203104.
(37) Chen, S.; Ji, D.; Chen, Q.; Ma, J.; Hou, S.; Zhang, J. Coordination modulation of hydrated zinc ions to enhance redox reversibility of zinc batteries. *Nat. Commun.* **2023**, *14* (1), 3526.
(38) Krossing, I.; Raabe, I. Noncoordinating anions-fact or fiction? A survey of likely candidates. *Angew. Chem., Int. Ed.* **2004**, *43* (16), 2066−2090.
(39) Horia, R.; Nguyen, D. T.; Eng, A. Y. S.; Seh, Z. W. Using a Chloride-Free Magnesium Battery Electrolyte to Form a Robust Anode-Electrolyte Nanointerface. *Nano Lett.* **2021**, *21* (19), 8220−8228.
(40) Chinnadurai, D.; Lieu, W. Y.; Kumar, S.; Yang, G.; Li, Y.; Seh, Z. W. A Passivation-Free Solid Electrolyte Interface Regulated by Magnesium Bromide Additive for Highly Reversible Magnesium Batteries. *Nano Lett.* **2023**, *23* (4), 1564−1572.
(41) Zheng, J.; Archer, L. A. Crystallographically Textured Electrodes for Rechargeable Batteries: Symmetry, Fabrication, and Characterization. *Chem. Rev.* **2022**, *122* (18), 14440−14470.
(42) Yang, G.; Li, Y.; Wang, J.; Lum, Y.; Lim, C. Y. J.; Ng, M.-F.; Zhang, C.; Chang, Z.; Zhang, Z.; Handoko, A. D.; et al. Realizing horizontal magnesium platelet deposition and suppressed surface passivation for high-performance magnesium metal batteries. *Energy Environ. Sci.* **2024**, *17*, 1141−1152.
(43) Zhang, X.; Li, J.; Liu, Y.; Lu, B.; Liang, S.; Zhou, J. Single [0001]-oriented zinc metal anode enables sustainable zinc batteries. *Nat. Commun.* **2024**, *15* (1), 2735.
(44) Tan, C.; Chen, J.; Wu, X.-J.; Zhang, H. Epitaxial growth of hybrid nanostructures. *Nat. Rev. Mater.* **2018**, *3* (2), 17089.
(45) Wang, G.; Liu, X.; Shi, H.; Ma, Y.; Wang, Z.; Sun, C.; Song, F.; Zhang, Z.; Dong, S.; Sun, M.; et al. Achieving Planar Electroplating/Stripping Behavior of Magnesium Metal Anode for a Practical Magnesium Battery. *ACS Energy Lett.* **2024**, *9* (1), 48−55.
(46) Tang, K.; Du, A.; Dong, S.; Cui, Z.; Liu, X.; Lu, C.; Zhao, J.; Zhou, X.; Cui, G. A Stable Solid Electrolyte Interphase for Magnesium Metal Anode Evolved from a Bulky Anion Lithium Salt. *Adv. Mater.* **2020**, *32* (6), No. e1904987.
(47) Long, J.; An, Y.; Yang, Z.; Zhang, G.; Zhang, J.; Tan, S.; An, Q. Efficient boron-based electrolytes constructed by anionic and interfacial co-regulation for rechargeable magnesium batteries. *Chem. Eng. J.* **2023**, *461*, 141901.

https://doi.org/10.1021/acsenergylett.4c02162
ACS Energy Lett. 2024, 9, 5019−5026